

Automatic Brain Tumor Segmentation with Scale Attention Network

Yading Yuan

Department of Radiation Oncology
Icahn School of Medicine at Mount Sinai
New York, NY, USA

Abstract. Automatic segmentation of brain tumors is an essential but challenging step for extracting quantitative imaging biomarkers for accurate tumor detection, diagnosis, prognosis, treatment planning and assessment. Multimodal Brain Tumor Segmentation Challenge 2020 (BraTS 2020) provides a common platform for comparing different automatic algorithms on multi-parametric Magnetic Resonance Imaging (mpMRI) in tasks of 1) Brain tumor segmentation MRI scans; 2) Prediction of patient overall survival (OS) from pre-operative MRI scans; 3) Distinction of true tumor recurrence from treatment related effects and 4) Evaluation of uncertainty measures in segmentation. We participate the image segmentation challenge by developing a fully automatic segmentation network based on encoder-decoder architecture. In order to better integrate information across different scales, we propose a dynamic scale attention mechanism that incorporates low-level details with high-level semantics from feature maps at different scales. Our framework was trained using the 369 challenge training cases provided by BraTS 2020, and achieved an average Dice Similarity Coefficient (DSC) of 0.8828, 0.8433 and 0.8177, as well as 95% Hausdorff distance (in millimeter) of 5.2176, 17.9697 and 13.4298 on 166 testing cases for whole tumor, tumor core and enhanced tumor, respectively, which ranked itself as the 3rd place among 693 registrations in the BraTS 2020 challenge.

1 Introduction

Gliomas are the most common primary brain malignancies and quantitative assessment of gliomas constitutes an essential step of tumor detection, diagnosis, prognosis, treatment planning and outcome evaluation. As the primary imaging modality for brain tumor management, multi-parametric Magnetic Resonance Imaging (mpMRI) provides various different tissue properties and tumor spreads. However, proper interpretation of mpMRI images is a challenging task not only because of the large amount of three-dimensional (3D) or four-dimensional (4D) image data generated from mpMRI sequences, but also because of the intrinsic heterogeneity of brain tumor. As a result, computerized analysis have been of great demand to assist clinicians for better interpretation of mpMRI images for brain tumor. In particular, the automatic segmentation of brain tumor and its sub-regions is an essential step in quantitative image analysis of mpMRI images.

The brain tumor segmentation challenge (BraTS) [1,2,3,4,5] aims to accelerate the research and development of reliable methods for automatic brain tumor segmentation by providing a large 3D mpMRI dataset with ground truth annotated by multiple physicians. This year, BraTS 2020 provides 369 cases for model training and 125 cases for model validation. The MRI scans were collected from 19 institutions and acquired with different protocols, magnetic field strengths and manufacturers. For each patient, a native T1-weighted, a post-contrast T1-weighted, a T2-weighted and a T2 Fluid-Attenuated Inversion Recovery (FLAIR) were provided. These images were rigidly registered, skull-stripped and resampled to $1 \times 1 \times 1$ mm isotropic resolution with image size of $240 \times 240 \times 155$. Three tumor subregions, including the enhancing tumor, the peritumoral edema and the necrotic and other non-enhancing tumor core, were manually annotated by one to four raters following the same annotation protocol and finally approved by experienced neuro-radiologists.

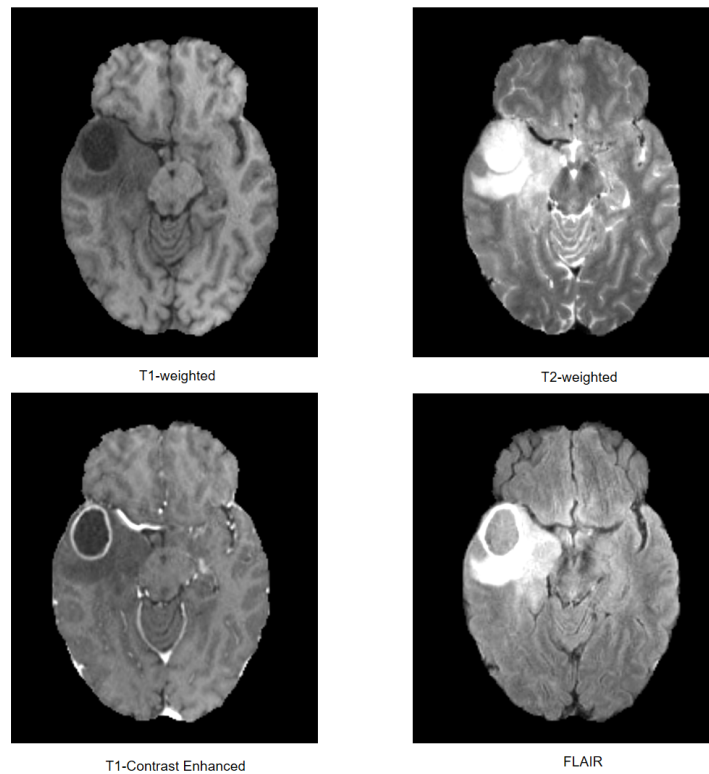


Fig. 1. An example of MRI modalities used in BraTS 2020 challenge

2 Related work

With the success of convolutional neural networks (CNNs) in biomedical image segmentation, all the top performing teams in recent BraTS challenges exclusively built their solutions around CNNs. In BraTS 2017, Kamnitsas et al. [6] combined three different network architectures, namely 3D FCN [7], 3D U-Net [9], and DeepMedic [8] and trained them with different loss functions and different normalization strategies. Wang et al. [10] employed a FCN architecture enhanced by dilated convolutions [11] and residual connections [12]. In BraTS 2018, Myronenko [13] utilized an asymmetrical U-Net with a large encoder to extract image features, and a smaller decoder to recover the label. A variational autoencoder (VAE) branch was added to reconstruct the input image itself in order to regularize the shared encoder and impose additional constraints on its layers. Isensee et al. [14] introduced various training strategies to improve the segmentation performance of U-Net. In BraTS 2019, Jiang et al. [15] proposed a two-stage cascaded U-Net, which was trained in an end-to-end fashion, to segment the subregions of brain tumor from coarse to fine, and Zhao et al. [16] investigated different kinds of training heuristics and combined them to boost the overall performance of their segmentation model.

The success of U-Net and its variants in automatic brain tumor segmentation is largely contributed to the skip connection design that allows high resolution features in the encoding pathway be used as additional inputs to the convolutional layers in the decoding pathway, and thus recovers fine details for image segmentation. While intuitive, the current U-Net architecture restricts the feature fusion at the same scale when multiple scale feature maps are available in the encoding pathway. Studies [17,18] have shown feature maps in different scales usually carry distinctive information in that low-level features represent detailed spatial information while high-level features capture semantic information such as target position, therefore, the full-scale information may not be fully employed with the scale-wise feature fusion in the current U-Net architecture.

To make full use of the multi-scale information, we propose a novel encoder-decoder network architecture named scale attention network (SA-Net), where we re-design the inter-connections between the encoding and decoding pathways by replacing the scale-wise skip connections in U-Net with full-scale skip connections. This allows SA-Net to incorporate low-level fine details with the high-level semantic information into a unified framework. In order to highlight the important scales, we introduce the attention mechanism [19,25] into SA-Net such that when the model learns, the weight on each scale for each feature channel will be adaptively tuned to emphasize the important scales while suppressing the less important ones. Figure 2 shows the overall architecture of SA-Net.

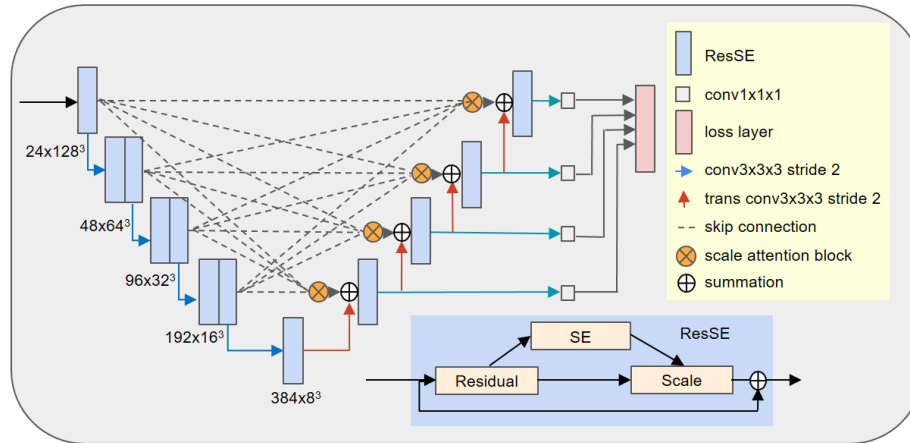


Fig. 2. Architecture of SA-Net. Input is a $4 \times 128 \times 128 \times 128$ tensor followed by one ResSE block with 24 features. Here ResSE stands for a squeeze-and-excitation block embedded in a residual module [19]. By progressively halving the feature map dimension while doubling the feature width at each scale, the endpoint of the encoding pathway has a dimension of $384 \times 8 \times 8 \times 8$. The output of the decoding pathway has three channels with the same spatial size as the input, i.e., $3 \times 128 \times 128 \times 128$.

3 Methods

3.1 Overall network structure

SA-Net follows a typical encoding-decoding architecture with an asymmetrically larger encoding pathway to learn representative features and a smaller decoding pathway to recover the segmentation mask in the original resolution. The outputs of encoding blocks at different scales are merged to the scale attention blocks (SA-block) to learn and select features with full-scale information. Due to the limit of GPU memory, we randomly crop the input image from $240 \times 240 \times 155$ to $128 \times 128 \times 128$, and concatenate the four MRI modalities of each patient into a four channel tensor to yield an input to SA-Net with the dimension of $4 \times 128 \times 128 \times 128$. The network output includes three channels, each of which presents the probability that the corresponding voxel belongs to *WT*, *TC*, and *ET*, respectively.

3.2 Encoding pathway

The encoding pathway is built upon ResNet [12] blocks, where each block consists of two Convolution-Normalization-ReLU layers followed by additive skip connection. We keep the batch size to 1 in our study to allocate more GPU memory resource to the depth and width of the model, therefore, we use instance normalization [24] that has been demonstrated with better performance than batch

normalization when batch size is small. In order to further improve the representative capability of the model, we add a squeeze-and-excitation module [19] into each residual block with reduction ratio $r = 4$ to form a ResSE block. The initial scale includes one ResSE block with the initial number of features (width) of 24. We then progressively halve the feature map dimension while doubling the feature width using a strided (stride=2) convolution at the first convolution layer of the first ResSE block in the adjacent scale level. All the remaining scales include two ResSE blocks except the endpoint of the encoding pathway, which has a dimension of $384 \times 8 \times 8 \times 8$. We only use one ResSE block in the endpoint due to its limited spatial dimension.

3.3 Decoding pathway

The decoding pathway follows the reverse pattern as the encoding one, but with a single ResSE block in each spatial scale. At the beginning of each scale, we use a transpose convolution with stride of 2 to double the feature map dimension and reduce the feature width by 2. The upsampled feature maps are then added to the output of SA-block. Here we use summation instead of concatenation for information fusion between the encoding and decoding pathways to reduce GPU memory consumption and facilitate the information flowing. The endpoint of the decoding pathway has the same spatial dimension as the original input tensor and its feature width is reduced to 3 after a $1 \times 1 \times 1$ convolution and a sigmoid function.

In order to regularize the model training and enforce the low- and middle-level blocks to learn discriminative features, we introduce deep supervision at each intermediate scale level of the decoding pathway. Each deep supervision subnet employs a $1 \times 1 \times 1$ convolution for feature width reduction, followed by a trilinear upsampling layer such that they have the same spatial dimension as the output, then applies a sigmoid function to obtain extra dense predictions. These deep supervision subnets are directly connected to the loss function in order to further improve gradient flow propagation.

3.4 Scale attention block

The proposed scale attention block consists of full-scale skip connections from the encoding pathway to the decoding pathway, where each decoding layer incorporates the output feature maps from all the encoding layers to capture fine-grained details and coarse-grained semantics simultaneously in full scales. As an example illustrated in Fig. 3, the first stage of the SA-block is to transform the input feature maps at different scales in the encoding pathway, represented as $\{S_e, e = 1, \dots, N\}$ where N is the number of total scales in the encoding pathway except the last block ($N = 4$ in this work), to a same dimension, i.e., $\tilde{S}_{ed} = f_{ed}(S_e)$. Here e and d are the scale level at the encoding and decoding pathways, respectively. The transform function $f_{ed}(S_e)$ is determined as follows. If $e < d$, $f_{ed}(S_e)$ downsamples S_e by $2^{(d-e)}$ times by maxpooling followed by

a Conv-Norm-ReLU block; if $e = d$, $f_{ed}(S_e) = S_e$; and if $e > d$, $f_{ed}(S_e)$ up-samples S_e through tri-linear upsampling after a Conv-Norm-ReLU block for channel number adjustment. After summing these transformed feature maps as $P_d = \sum_e \bar{S}_{ed}$, a spatial pooling is used to average each feature to form an information embedding tensor $G_d \in R^{C_d}$, where C_d is the number of feature channels in scale d . Then a $1 - to - N$ Squeeze-Excitation is performed in which the global feature embedding G_d is squeezed to a compact feature $g_d \in R^{C_d/r}$ by passing through a fully connected layer with a reduction ratio of r , then another N fully connected layers with sigmoid function are applied for each scale excitation to recalibrate the feature channels on that scale. Finally, the contribution of each scale in each feature channel is normalized with a softmax function, yielding a scale-specific weight vector for each channel as $w_e \in R^{C_d}$, and the final output of the scale attention block is $\tilde{S}_d = \sum_e w_e \cdot \bar{S}_{ed}$.

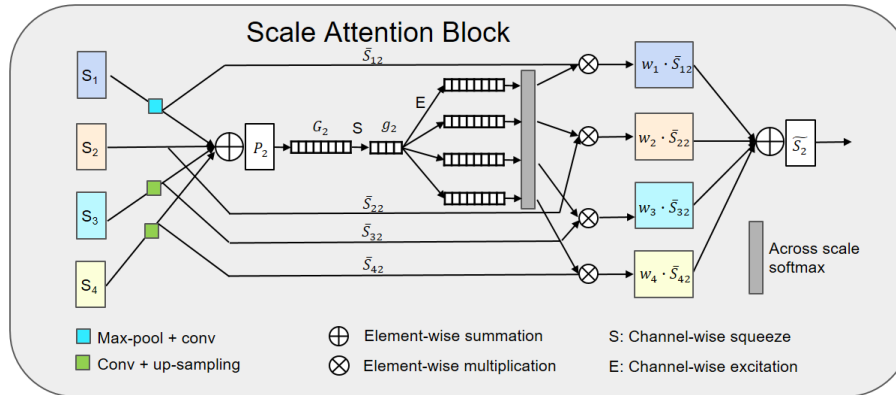


Fig. 3. Scale attention block. Here S_1, S_2, S_3 and S_4 represent the input feature maps at different scales from the encoding pathway. $d = 2$ in this example.

3.5 Implementation

Our framework was implemented with Python using Pytorch package. As for pre-processing, since MRI images are non-standardized, we simply normalized each modality from each patient independently by subtracting the mean and dividing by the standard deviation of the entire image. The model was trained with randomly sampled patches of size $128 \times 128 \times 128$ voxels and batch size of 1. Training the entire network took 300 epochs from scratch using Adam stochastic optimization method. The initial learning rate was set as 0.003, and learning rate decay and early stopping strategies were utilized when validation loss stopped decreasing. In particular, we kept monitoring both the validation loss ($L^{(valid)}$) and the exponential moving average of the validation loss ($\tilde{L}^{(valid)}$)

in each epoch. We kept the learning rate unchanged at the first 150 epochs, but dropped the learning rate by a factor of 0.3 when neither $L^{(valid)}$ nor $\tilde{L}^{(valid)}$ improved within the last 30 epochs. The models that yielded the best $L^{(valid)}$ and $\tilde{L}^{(valid)}$ were recorded for model inference.

Our loss function used for model training includes two terms:

$$L = L_{jaccard} + L_{focal} \quad (1)$$

$L_{jaccard}$ is a generalized Jaccard distance loss [20,21,22,23], which we developed in our previous work for single object segmentation, to multiple objects, and L_{focal} is the voxel-wise focal loss function that focuses more on the difficult voxels. Since the network output has three channels corresponding to the whole tumor, tumor core and enhanced tumor, respectively, we simply added the three loss functions together.

In order to reduce overfitting, we randomly flipped the input volume in left/right, superior/inferior, and anterior/posterior directions on the fly with a probability of 0.5 for data augmentation. We also adjusted the contrast in each image input channel by a factor randomly selected from [0.9, 1.1]. We used 5-fold cross validation to evaluate the performance of our model on the training dataset, in which a few hyper-parameters were also experimentally determined. All the experiments were conducted on Nvidia GTX 1080 TI GPU with 11 GB memory.

During testing, we applied the sliding window around the brain region and extracted 8 patches with a size $128 \times 128 \times 128$ (2 windows in each dimension), and averaged the model outputs in the overlapping regions before applying a threshold of 0.5 to obtain a binary mask of each tumor region.

4 Results

We trained SA-Net with the training set (369 cases) provided by the BraTS 2020 challenge, and evaluated its performance on the training set via 5-fold cross validation, as well as on the validation set, which includes 125 cases with unknown segmentation. Table 1 shows the segmentation results in terms of Dice similarity coefficient (DSC) for each region. As compared to the results that were obtained from a model using the vanilla U-Net structure with scale-wise skip connection and feature concatenation, the proposed SA-Net consistently improved segmentation performance for each target, yielding an average 1.47% improvement.

When applying the trained models on the challenge validation dataset, a bagging-type ensemble strategy was implemented to combine the outputs of eleven models obtained through 5-fold cross validation to further improve the segmentation performance. In particular, our model ensemble included the models that yielded the best $L^{(valid)}$ (validation loss) and $\tilde{L}^{(valid)}$ (moving average of the validation loss) respectively in each fold, plus the model that was trained with all the 369 cases. We uploaded our segmentation results to the BraTS 2020

Table 1. Comparison between SA-Net and U-Net segmentation results (DSC) in 5-fold cross validation using 369 training image sets. WT: whole tumor; TC: tumor core; ET: enhanced tumor.

		fold-0	fold-1	fold-2	fold-3	fold-4	ALL
SA-Net	WT	0.9256	0.9002	0.9217	0.9085	0.9195	0.9151
	TC	0.8902	0.8713	0.8758	0.8538	0.8953	0.8773
	ET	0.8220	0.7832	0.8198	0.8107	0.8268	0.8125
	AVG	0.8793	0.8516	0.8724	0.8577	0.8805	0.8683
U-Net	WT	0.9218	0.9003	0.9104	0.9021	0.9113	0.9092
	TC	0.8842	0.8735	0.8772	0.8307	0.8700	0.8671
	ET	0.7982	0.7672	0.7922	0.7955	0.8007	0.7908
	AVG	0.8680	0.8470	0.8599	0.8428	0.8607	0.8557

server for performance evaluation in terms of DSC, sensitivity, specificity and Hausdorff distance for each tumor region, as shown in Table 2.

Table 2. Segmentation results of SA-Net on the BraTS 2020 validation sets in terms of Mean DSC and 95% Hausdorff distance (mm). WT: whole tumor; TC: tumor core; ET: enhanced tumor.

	DSC			HD95		
	WT	TC	ET	WT	TC	ET
The best single model	0.9044	0.8422	0.7853	5.4912	8.3442	20.3507
Ensemble of 11 models	0.9108	0.8529	0.7927	4.0975	5.8879	18.1957

During the testing phase, only one submission was allowed. Table 3 summarizes our final results, which ranked our method as the 3rd place among 693 registrations in Brats 2020 challenge.

Table 3. Segmentation results of SA-Net on the BraTS 2020 testing sets in terms of Mean DSC and 95% Hausdorff distance (mm). WT: whole tumor; TC: tumor core; ET: enhanced tumor.

	DSC			HD95		
	WT	TC	ET	WT	TC	ET
Ensemble of 11 models	0.8828	0.8433	0.8177	5.2176	17.9697	13.4298

5 Summary

In this work, we presented a fully automated segmentation model for brain tumor segmentation from multimodality 3D MRI images. Our SA-Net replaces the long-range skip connections between the same scale in the vanilla U-Net with

full-scale skip connections in order to make maximum use of feature maps in full scales for accurate segmentation. Attention mechanism is introduced to adaptively adjust the weights of each scale feature to emphasize the important scales while suppressing the less important ones. As compared to the vanilla U-Net structure with scale-wise skip connection and feature concatenation, the proposed scale attention block not only improved the segmentation performance by 1.47%, but also reduced the number of trainable parameters from 17.8M (U-Net) to 16.5M (SA-Net), which allowed it to achieve a top performance with limited GPU resource in this challenge.

Acknowledgment

This work is partially supported by a research grant from Varian Medical Systems (Palo Alto, CA, USA) and grant UL1TR001433 from the National Center for Advancing Translational Sciences, National Institutes of Health, USA.

References

1. Menze, B.H. et al. The multimodal brain tumor image segmentation benchmark (BRATS). *IEEE Trans. Med. Imaging*, 34(10), 1993-2024, 2015.
2. Bakas, S. et al. Advancing the cancer genome atlas glioma MRI collections with expert segmentation labels and radiomic features. *Nature Scientific Data*, 4:170117, 2017.
3. Bakas, S. et al. Identifying the best machine learning algorithms for brain tumor segmentation, progression assessment, and overall survival prediction in the BRATS challenge. *arXiv preprint arXiv:1811.02629*, 2018.
4. Bakas, S. et al. Segmentation labels and radiomic features for the pre-operative scans of the TCGA-GBM collection. *The Cancer Imaging Archive*, 2017.
5. Bakas, S. et al. Segmentation labels and radiomic features for the pre-operative scans of the TCGA-LGG collection. *The Cancer Imaging Archive*, 2017.
6. Kamnitsas, K. et al. Ensembles of multiple models and architectures for robust brain tumor segmentation. in *BrainLes 2017. LNCS*, vol. 10670, 450-462, 2018.
7. Long, J. et al. Fully convolutional networks for semantic segmentation. *CVPR*, 3431-3440, 2015
8. Kamnitsas, K. et al. Efficient multi-scale 3D CNN with fully connected CRF for accurate brain lesion segmentation. *Medical Image Analysis*, 36, 61-78, 2017.
9. Ronneberger, O. et al. U-Net: Convolutional networks for biomedical image segmentation. in *Proc. MICCAI 2015*. Springer, 234-241, 2015.
10. Wang, G. et al. Automatic brain tumor segmentation using cascaded anisotropic convolutional neural networks. In *BrainLes 2018 LNCS*, vol. 10670, 178-190, 2018
11. Chen, L.-C., et al. DeepLab: semantic image segmentation with deep convolutional nets, atrous convolution, and fully connected CRFs. *IEEE Trans. Pattern Anal. Mach. Intell.*, 40(4), 834-848, 2018
12. He, K. et al. Deep residual learning for image recognition. In *proc. CVPR 2016*, 770-778, 2016.
13. Myronenko, A., et al. 3D MRI brain tumor segmentation using autoencoder regularization. In *BrainLes 2018. LNCS*, vol. 11384, 311 - 320, 2019.

14. Isensee, F. et al. No new-net. In BrainLes 2018. LNCS, vol 11384, 234-244, 2019.
15. Jiang, Z. et al. Two-stage cascaded U-Net: 1st place solution to BraTS Challenge 2019 segmentation task. BrainLes 2019, LNCS vol 11992, 231 - 241, 2020
16. Zhao, Y. et al. Bag of tricks fo 3D MRI brain tumor segmentation. BrainLes 2019, LNCS vol 11992, 210 - 220, 2020.
17. Zhou, Z. et al. Unet++: redesigning skip connections to exploit multiscale features in image segmentation. IEEE Trans. Med. Imaging, 39(6), 1856-1867, 2019.
18. Roth, H, et al. Spatial aggregation of holistically-nested convolutional neural networks for automated pancreas localization and segmentation. Med. Imag. Anal. 45, 94-107, 2018.
19. Hu, J. et al. Squeeze-and-excitation networks. In proc. CVPR 2018, 7132-7141, 2018.
20. Yuan, Y. et al. Automatic skin lesion segmentation using deep fully convolutional networks with Jaccard distance. IEEE Trans. Med. Imaging, 36(9), 1876-1886, 2017.
21. Yuan, Y. Hierarchical convolutional-deconvolutional neural networks for automatic liver and tumor segmentation. arXiv preprint arXiv:1710.04540, 2017.
22. Yuan, Y. Automatic skin lesion segmentation with fully convolutional-deconvolutional networks. arXiv preprint arXiv:1703.05154, 2017.
23. Yuan, Y., et al. Improving dermoscopic image segmentation with enhanced convolutional-deconvolutional networks. IEEE J. Biomed. Health Informat., 23(2), 519-526, 2019.
24. Wu, Y. et al. Group normalization. In proc. ECCV 2018, 3-19, 2018.
25. Li, X. et al. Selective kernel networks. In proc. CVPR 2019, 510-519, 2019